

Effect of indentation unloading conditions on phase transformation induced events in silicon

Tom Juliano, Yury Gogotsi,^{a)} and Vladislav Domnich

Department of Materials Engineering, Drexel University, Philadelphia, Pennsylvania 19104

(Received 6 September 2002; accepted 19 February 2003)

More than 2500 indentations were made on a silicon wafer surface using a range of different unloading rates and maximum applied loads. The unloading curves were examined for characteristic events (pop-out, kink pop-out, elbow followed by pop-out, and elbow) that were assigned to different phase transitions within the affected material based on Raman microspectroscopy analysis of residual imprints. The effect of unloading rate and maximum applied load on the average contact pressure at the beginning of the event was found. A permissible range for each event to occur was established.

I. INTRODUCTION

The response of single-crystal silicon to loading and unloading during indentation has been widely researched during the past decade.¹ It has been established that discontinuities in its load–displacement curve under various loading conditions appear, referred to as pop-in and pop-out events.^{1–3} The pop-in event in silicon has been seen for spherical indentations^{2,4} but has never been reported for indentations created by sharp tools. The pop-out event has been seen for both spherical and sharp indentation, however.^{2,4,5} Furthermore, the influence of a size effect for this phenomena within the microscale has been shown to not exist.⁶ These events have also been seen to occur multiple times in unloading curves during cyclic loading conditions.⁷

It was suggested that the pop-in event for spherical indenters is the result of a phase change from cubic-diamond Si-I to metallic β -tin Si-II,^{2,8} which is known to occur between 11.3 and 12 GPa under hydrostatic loading in high-pressure cells.^{9,10} The pop-in discontinuity is reasoned to occur because there is a sudden volume change when this critical pressure is reached, as the volume decrease from Si-I to Si-II is about 22%. This transition would be at an extremely low load for sharp indenters because the contact pressure quickly exceeds this critical value, and the transformation to Si-II occurs at shallow depths, starting from the very beginning stages of the indentation if the indenter is perfectly sharp. However, the pop-in discontinuity has also been found for Fe–3 wt.% Si and other materials and has been shown to be caused by yielding by dislocation nucleation.¹¹ For

sharp indenters, these pop-in effects have routinely been found at loads below about 2 mN. For the case of a pop-out event, it has been suggested that the pressurized Si-II phase suddenly transforms upon unloading into the rhombohedral r8 (Si-XII) phase. This is based on transmission electron microscopy (TEM) and Raman analysis of the residual imprints.^{5,8,12,13} It is known that the Si-II to Si-III phase change is accompanied by a 9% increase in volume. Upon further decompression, Si-XII transforms gradually into the body-centered-cubic bc8 (Si-III) phase according to high-pressure cell data.¹⁴

It was experimentally found that the resulting Si-III and Si-XII formed during slower unloading rates that yielded pop-outs, and a-Si formed during faster unloading rates^{5,13} when the unloading curve “elbowed” and showed a continual change in curvature that could not be fit by a power-law relation, such as that shown in Figs. 1 and 2. It is important to realize that the elbow behavior in the silicon unloading curve is not like that found in many other brittle materials at the load range that was examined (15–105 mN). However, certain materials such as thin carbon surfaces have been shown to produce elbowing behavior in their unloading curves.¹⁵ When this happens, it may serve as evidence that phase transformations are occurring during unloading in these materials as well. At the micro-Newton level there has been an elbowing effect seen in materials such as aluminum when performing nanoindentation with an atomic force microscope.¹⁶ An illustration of an elbow in the silicon unloading curve with a maximum load of 10 mN compared with other brittle materials at similar loading and unloading conditions can be seen in Fig. 1. Note that if silicon behaved in a similar manner to the other materials, its unloading curve would follow the dotted line path instead.

^{a)}Address all correspondence to this author.

Currently, there has been only limited work done to classify the contact pressures and frequency of events that take place during unloading. Zarudi and Zhang¹⁷ have done some work for a spherical indenter, finding depths of transformed zones for different loads; however, an extensive statistical analysis was not performed. No systematic and statistically significant study of the effect of maximum load and the unloading rate on the phase-transformation-induced changes on the shape of load–displacement curves has ever been conducted. In this research, we set out to find the response of silicon to various maximum applied loads (15–105 mN) and unloading rates (1–30 nm/s) for

Berkovich (three-sided pyramid) indentation. The effect of load and unloading rate on pop-out and elbow pressure will be examined, as well as permissible pressure ranges for these events.

II. EXPERIMENTAL

A Nano Indenter XP (MTS Systems) was used to create all indentations at ambient conditions. The 7×7 square arrays of indentations (Fig. 3) were placed on the surface of the same polished *p*-type (111) silicon wafer 1 mm thickness to ensure homogeneity of testing conditions. The indentations were placed 20 μm apart, and arrays were at least 500 μm apart from each other. Each indentation was made using a Berkovich diamond tool with an effective tip radius of about 100 nm. The sample and indentation tool maintained the same orientation to each other throughout the creation of all arrays, with the indented triangle shape optically symmetric to the (01 $\bar{1}$) plane with optical accuracy. A total of 54 arrays were created, yielding 2646 indentations that were used in the data sets. Each array contained indentations that had the same loading conditions in terms of maximum applied load and unloading rate.

The arrays differed from one another in maximum applied load and unloading rate. The unloading rate was determined in the following manner. The maximum

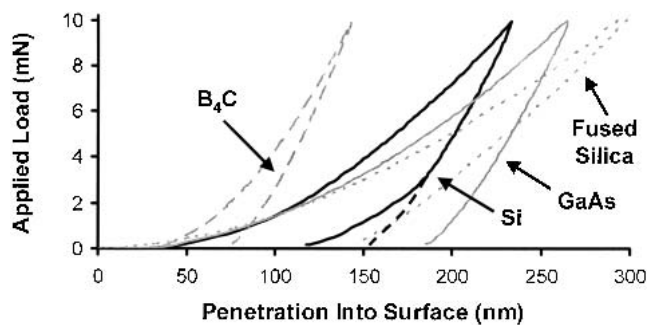


FIG. 1. Loading and unloading curves for boron carbide, silicon, gallium arsenide, and fused silica at a maximum applied load of 10 mN, illustrating the presence of the elbow event in silicon.

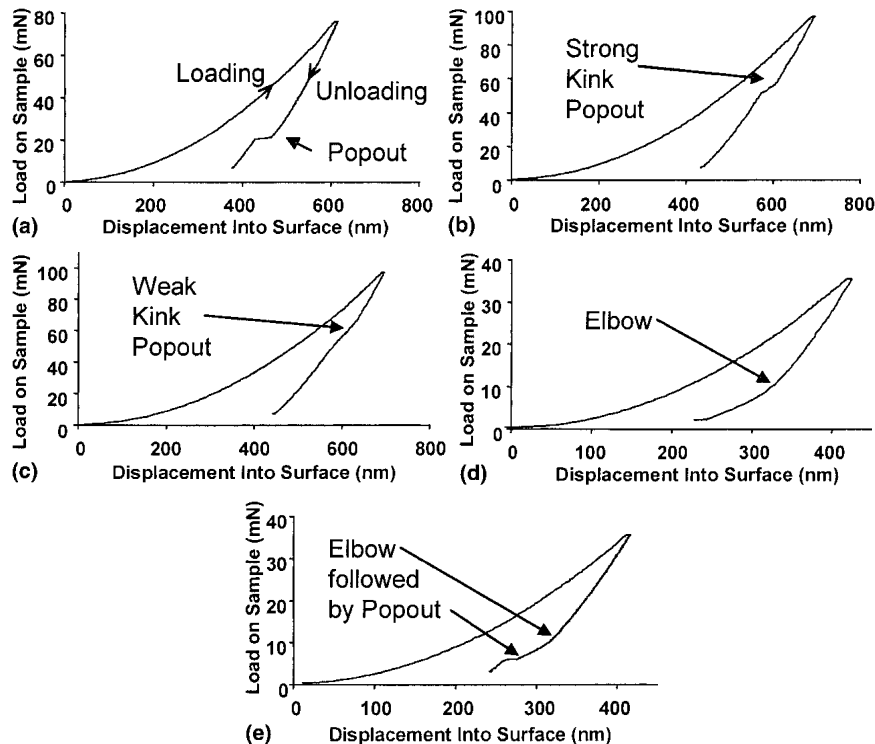


FIG. 2. Classification of different typical unloading curves for the (a) pop-out, (b) strong kink pop-out, (c) weak kink pop-out, (d) elbow events in silicon, and (e) elbow followed by pop-out.

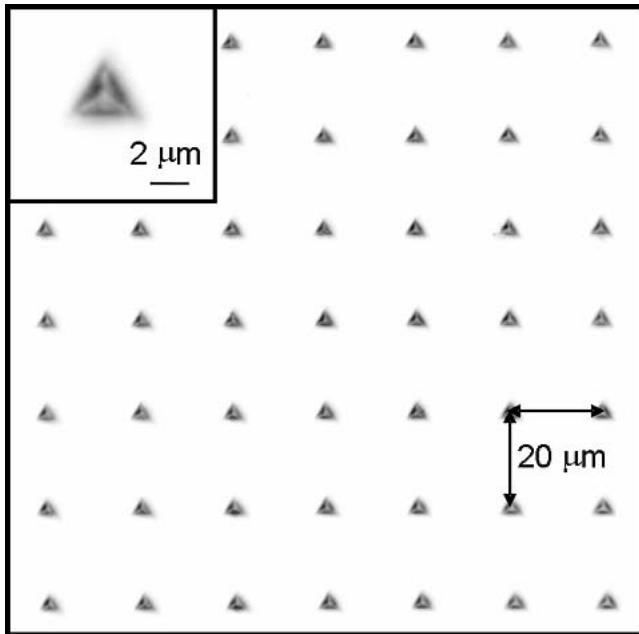


FIG. 3. Inverted dark-field optical micrograph of an array of indentations with a maximum applied load of 95 mN.

indentation depth as a function of maximum applied load on silicon was determined experimentally to fit the linear equation within the load range of 15–105 mN:

$$d = 4.76 p + 260.5 \quad (1)$$

where d is the maximum indentation depth in nm, and p is the known maximum applied load in mN. We then introduced an average unloading rate U that could roughly be correlated to the unloading velocity, and is defined as

$$U = d/t \text{ (nm/s)} \quad (2)$$

where t is the total unloading time in seconds. This average unloading rate was set to be integer values ranging from 1 to 30 nm/s in these experiments. Because the shapes of the loading and unloading curves for silicon are similar in the range of 15–105 mN, it is expected that the velocity and the strain rate of the tool–material interface is constant during unloading for the same average unloading rate and different maximum applied loads in this load range.

All indentations performed had the same loading time of 30 s and the same holding time at the maximum load, to account for creep, of 30 s. Load–displacement data were taken in each case until 90% of unloading was complete. Thirty arrays were made by holding the average unloading rate constant to 2, 3, or 4 nm/s while varying the maximum applied load from 15 to 105 mN in steps of 10 mN. Twenty-four arrays were made by holding the maximum applied load constant at 35, 75, or 95 mN, and then varying the average unloading rate to be either 1, 2, 3, 4, 5, 10, 20, or 30 nm/s. Subsequently, for

all indentations made, load and displacement data were gathered by the Nano Indenter and analyzed after tests were completed. These loading conditions were chosen such that we would obtain a sufficient amount of elbows and pop-outs for statistical analysis based on previous experience.

A Ramascope 1000 Raman microspectrometer (Renishaw Inc., United Kingdom) was used to identify phases inside the indented area (namely Si-I, Si-III, Si-XII, and a-Si) after all tests were completed. Fifty indentations exhibiting a range of different events were checked for phase composition using the 514.5-nm wavelength of a green argon ion laser, detecting to about a 0.8- μm depth into the Si-I surface. Fifty indentations were similarly checked using the 633-nm wavelength of the red helium-neon laser, detecting to about a 3- μm depth into the Si-I surface. The reason two different lasers were used was to see if different phases are present at different material depths. The effective spot size diameter of the focused laser beam in each case was about 2 μm , and the time for collecting each spectrum was at least 30 s, sometimes longer to obtain clear spectra.

The pressures the events took place at were calculated using the elastic recovery contact mechanics methods of Oliver and Pharr¹⁸ and Novikov *et al.*¹⁹ To calculate the event pressures, the average contact pressure at the beginning of the event was evaluated by the following method.

The average contact pressure at a certain point σ_i between the indenter tool and the sample is defined as

$$\sigma_i = \frac{P_i}{A_i} \quad (3)$$

where P_i is the applied load, and A_i is the projected contact area at time i . We may directly get the value of the applied load by consulting the gathered load–displacement data.

To find the contact area, we consider the elastic deflection of the material at the perimeter of the indentation area at the time the event occurs. First, the elastic deflection at maximum load $(h_s)_{\text{max}}$ is calculated using the following equation:¹⁸

$$(h_s)_{\text{max}} = \epsilon \frac{P_{\text{max}}}{S} \quad (4)$$

where ϵ is a geometrical constant equal to 0.75, P_{max} is the maximum measured load applied on the sample, and S is the stiffness of the sample measured at the beginning of unloading.

Second, the elastic deflection at a point, $(h_s)_i$, is determined by using the relation between the indentation depth and load obtained from contact mechanics:²⁰

$$(h_s)_i = (h_s)_{\text{max}} \sqrt{\frac{P_i}{P_{\text{max}}}} \quad (5)$$

Next, we know that the depth of the material that is in contact with the tool (h_c)_{*i*} is:¹⁸

$$(h_c)_i = h_i - (h_s)_i \quad (6)$$

where h_i is the indenter displacement at point i measured experimentally. Last, the value of A_i is calculated by the expression:

$$A_i = 24.5(h_c)_i^2 + \sum_{i=1}^7 C_i h_c^{1/2^i} \quad (7)$$

where C_i is a constant experimentally found to describe the imperfect tip geometry of the three-sided Berkovich pyramidal indenter used for these experiments. Note that the values of C_i contribute less to the contact area as the indenter depth increases. Now, the average contact pressure can be directly calculated at the moment the event takes place.

III. RESULTS AND DISCUSSION

A. Classification of indentation curves

After the indentations were made, each load-displacement curve was carefully examined. There were four classifications made to distinguish the observed shape and derivative of the unloading portion of the curve for each type of event. These are pop-out, kink pop-out [which can be less (weak) or more (strong) pronounced], elbow followed by pop-out, and elbow events. An example of each of these classifications can be seen in Fig. 2.

For a curve to be classified as having a pop-out event [Fig. 2(a)], the unloading curve must maintain a constant curvature until the event, which occurs when the indenter suddenly gets pushed up by the expanding silicon. On pop-out curves, there is always a pronounced plateau

where the silicon volume change occurs, and the segment of the curve thereafter will exhibit a constant curvature. When taking the derivative dh/dP of a pop-out unloading curve, on the onset of the event, the derivative suddenly increases several orders of magnitude and then returns to the lower curve. These particular features are unique for pop-out events. An example of the unloading curve derivative for a pop-out event is illustrated in Fig. 4(a).

Curves classified as having kink pop-out events exhibit a constant curvature up until the point where the pop-out starts, but the kink pop-out happens during a broader unloading segment and a longer time span than the regular pop-out. The kink pop-out curve will return to a curve with constant curvature and has the distinctive shape in its unloading curve aesthetically appearing as a twist or a kink in a hose, like a spline function. Examples of strong and weak kink pop-outs are shown in Figs. 2(b) and 2(c). When taking the derivative dh/dP for these events as a function of depth, one finds that similar to a pop-out event, the derivative slowly and then suddenly increases during the event. However, for a kink pop-out, this change is much weaker than for a pop-out, and the derivative during the event is on the order of 5–10 nm/mN or lower. An example of the unloading curve derivative for a kink pop-out event is illustrated in Fig. 4(b).

Curves classified as elbow [Fig. 2(d)] are marked by having a smooth and accelerated curvature (second derivative) change at the onset of the event. When taking the derivative dh/dP for a curve exhibiting an elbow event, one finds that as a function of depth it slowly increases at first and begins to deviate from power-law curve fitting²¹ at the onset of the event. This event usually continues until the end of the entire unloading segment. An example of the unloading curve derivative for an elbow event and its deviation from a power-law curve fit is shown in Fig. 4(c).

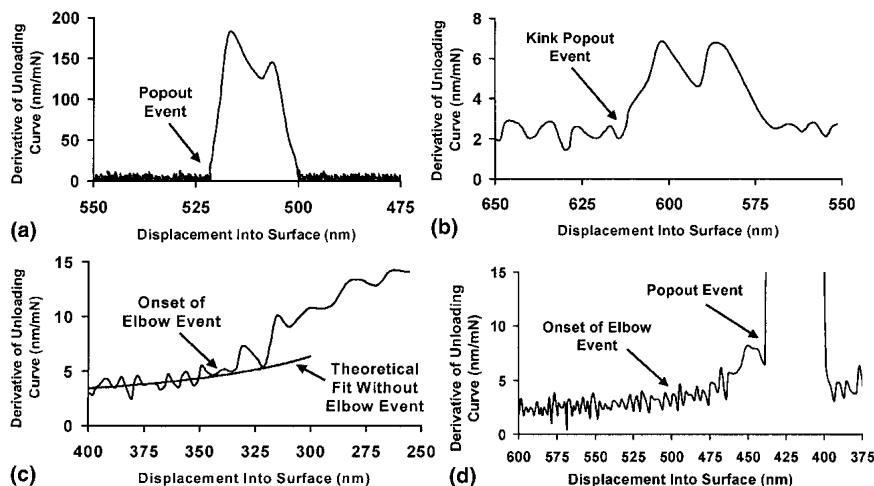


FIG. 4. Derivative of the unloading curve as a function of penetration depth for (a) pop-out, (b) kink pop-out, (c) elbow, and (d) elbow followed by pop-out events.

Last, for a curve to be classified as having an elbow followed by a pop-out event (or just elbow pop-out events), upon unloading is first marked as having a smooth and continuous curvature change characteristic of an elbow. After this behavior, at a certain instant, the material suddenly expands and the plateau characteristic of a pop-out is seen [Fig. 2(e)]. To be classified as an elbow followed by pop-out, the derivative behavior then must necessarily have the feature of having first a gradually increasing derivative, then a steeper increase rate, followed by a sudden increase to the range of about 100–200 nm/mN and then back to the previous derivative level. An example of this behavior is shown in Fig. 4(d).

In summary, all four different unloading curve types exhibit different behavior in their unloading curves and in the derivative behavior of their unloading curves. Pop-out-associated events are relatively sudden, and the derivative at the place of the event is immediately significantly higher. Elbow-associated events take place over a longer portion of the unloading curve and the derivative change for these events sufficiently increases at the start of the event and continues to do so until the end of the unloading segment.

B. Calculation of event pressures

The aforementioned method was used to calculate pressures of all events in the data. For the clean pop-out, kink pop-out, and elbow events, load and displacement were noted at the instant a curvature change began. For the case of the elbow pop-out, the point where the pop-out began, not the elbow, was used to calculate event pressure. This point will admittedly fall below the pressure where amorphous phase transformation first occurs, however for the analysis at hand we are concerned with the pop-out pressure only.

At this point, one can plot the dependence of contact pressure on indentation depth throughout the course of the loading and unloading cycle. It is seen in Fig. 5 that the pressure at the beginning of the unloading segment is above 12 GPa (corresponding to the hardness of silicon) for any maximum indentation load. This is slightly above the accepted value needed for the Si-I to Si-II phase transformation to take place, which is between 11.3 and 12 GPa.⁹ This is evidence that at the beginning of unloading there will be a sufficient amount of Si-II under the indenter tip. Upon unloading, the pop-out and elbow events can be seen to affect subsequent pressure release in different manners, with post-pop-out pressure decreasing at a much faster rate than post-elbow pressure (Fig. 5).

C. Raman microspectroscopy

Three different types of spectrum were seen in the Raman analysis of the immediate indentation areas (Fig. 6). The first spectrum in Fig. 6(a) shows a strong

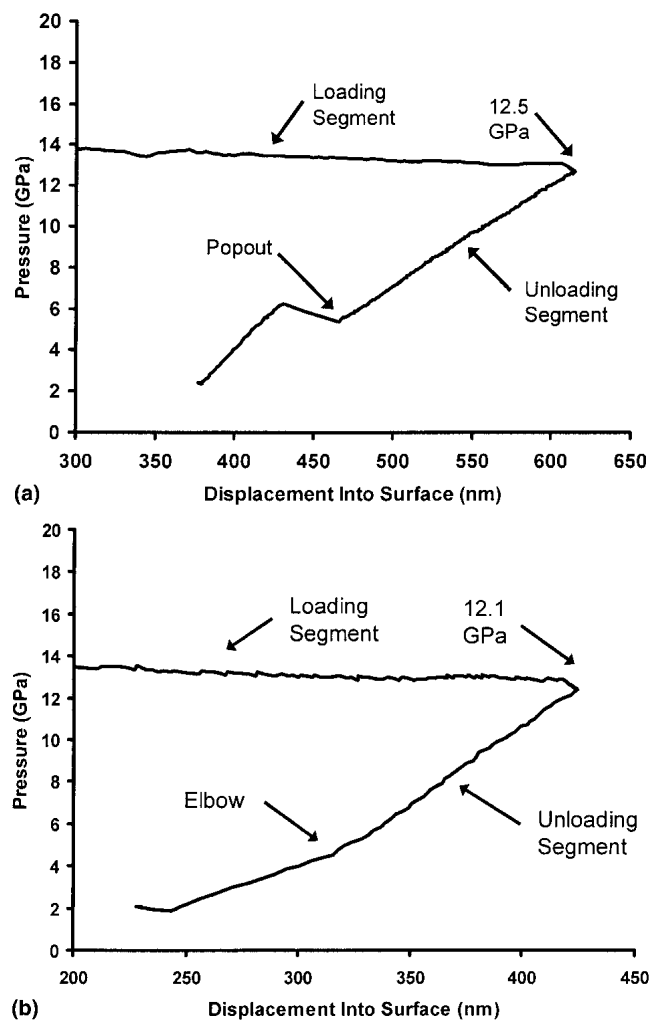


FIG. 5. Pressure dependence on displacement into surface for (a) pop-out and (b) elbow events at 75 and 35 mN, respectively.

presence of Si-III and Si-XII. Raman bands at 166, 382, and 433 cm^{-1} have been attributed to the presence of Si-III, and bands at 184, 350, 394, and 485 cm^{-1} are major bands of Si-XII.^{1,13,22} The third spectrum in Fig. 6(c) shows a strong presence of amorphous silicon. The characteristic bands of amorphous silicon are broad peaks around 170, 300, 390, and 470 cm^{-1} . The second spectrum in Fig. 6(b) shows a mixture of the two. In all spectra, there is still a strong presence of the 520 cm^{-1} peak, representative of the cubic diamond phase of silicon, Si-I, which surrounds the indentation area. A variation of this peak position is due to residual stresses around the indentation area.

For indentations with different kinds of unloading events, spectra were separated into these three representative categories. A summary of observed phases in the Raman spectra for different events can be found in Table I. The results for the 514.5 nm excitation wavelength laser were found to be in general agreement with work we have done previously.⁵ About 78% of

indentations inspected that exhibited pop-out and kink pop-out events showed a presence of only Si-III and Si-XII in their spectra, while the other 22% showed a presence of Si-III, Si-XII, and a-Si. This was the case for both the 514.5- and 633-nm lasers. It should be noted that laser light is much more easily absorbed by a-Si by about a factor of ten, as compared to Si-I.²³ Therefore, penetration depths in all cases are in fact somewhere in the range of 0.1–0.2 and 0.5–1.0 μm for the 514.5- and 633-nm lasers, respectively.

Almost identical phase compositions for indentations exhibiting pop-out and strong and weak kink pop-out events show that these events result from the same kind of phase transformation and can be grouped together. For elbow followed by pop-out and elbow events, the presence of phases found in Raman spectra was dependent on laser penetration depth. For the 514.5-nm laser, only a-Si was found in the majority of spectra, in agreement with Ref. 5, and for the 633-nm laser, a majority of spectra

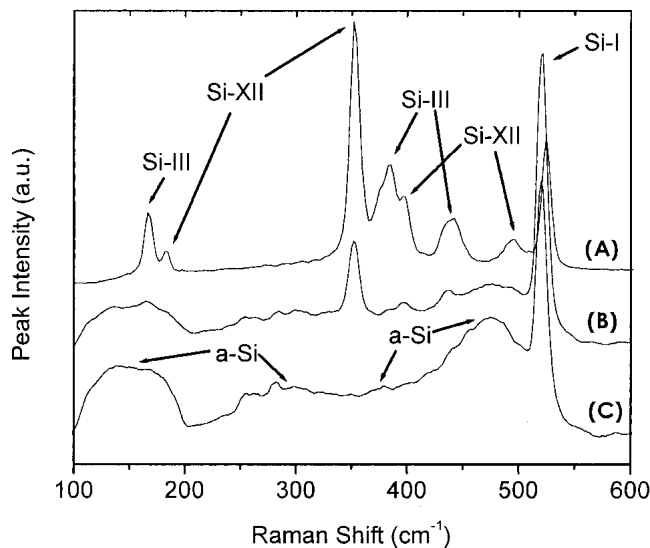


FIG. 6. Representative spectra of (a) Si-III and Si-XII phases, (b) a mixture of a-Si, Si-III, and Si-XII, and (c) a-Si experimentally found inside silicon nanoindentations.

showed a presence of a-Si, Si-III, and Si-XII. Indeed, this points to the fact that for elbow followed by pop-out and elbow events, there is a shallow layer of a-Si on the surface of the indenter, but Si-III and Si-XII exist underneath this layer. This type of configuration has been seen before. It has been found in cross-sectional TEM analysis after indentation with a spherical tool on a (100) orientation silicon wafer.¹⁷ This configuration has also been found for dynamic loading conditions on silicon²⁴ and only amorphous silicon was found on the outermost layer of crystalline silicon powders that had been subjected to ball milling, with transformed nanocrystalline particles inside.²⁵

D. Average event pressures for different maximum loads

Results were obtained for event pressures for varying maximum applied indentation load from 15 to 105 mN and average unloading rates of 2, 3, and 4 nm/s. It was found that for pop-out events, as maximum applied load increases for a given unloading factor, the average pop-out pressure also increases in a linear fashion for the load range in question. The results for the average unloading rate of 4 nm/s can be found in Fig. 7, and the results for 2 and 3 nm/s showed a similar trend. It can be seen in Fig. 7 that the average pop-out pressure raises from 4.76 GPa for a maximum applied load of 15 mN to 8.10 GPa for a maximum applied load of 105 mN. Because the transformed area of Si-I to pressurized Si-II is greater in higher load indentations, there is a higher chance of a new phase to nucleate since the pop-out event is a statistical process. Event frequencies for given loads can be seen in Fig. 8, and for a 95-mN indentation the contact area is on the order of 6 μm^2 . Through all unloading conditions, there was found to be a 100% chance of a kink or clean pop-out. However, for a 35-mN indentation, the chance to get a kink or clean pop-out event at higher unloading rates went down to about 50% with the contact area on the order of 2 μm^2 . Thus, we see that at higher loads, and consequently at

TABLE I. Phases detected in Raman spectra for different indentation events for laser penetration depths of 0.1–0.2 and 0.5–1 μm .

Phases detected in Raman spectra	Number of unloading curves showing				
	Pop-out	Weak kink pop-out	Strong kink pop-out	Elbow pop-out	Elbow
633 nm laser (penetration depth 0.5–1 μm)					
Si-III, Si-XII	8	8	7	0	0
Si-III, Si-XII, a-Si	2	2	3	10	7
a-Si	0	0	0	0	3
514.5 nm laser (penetration depth 0.1–0.2 μm)					
Si-III, Si-XII	9	8	7	0	0
Si-III, Si-XII, a-Si	1	2	3	2	3
a-Si	0	0	0	8	7

higher surface areas of transformed Si-II, the chance of obtaining a kink or clean pop-out event increases. According to Raman analysis results, this means that the chance of having Si-III and Si-XII on the surface of the indent goes to 100% above about 75 mN for a Berkovich indentation within the bounds of the variables tested. For the lower loads at a similar average unloading rate, this means that there will be a greater chance for amorphous silicon on the surface of the indentations because elbow events are much more probable.

It is useful and curious to note the average pressures at which all events occur, and results for the 4 nm/s average unloading rate are shown in Fig. 9. The same trends were seen for the 2 and 3 nm/s average unloading rate. If we separate the types of pop-out events we are obtaining for various maximum applied loads, we see that different

events are responsible for this shift. At lower loads (15–75 mN), we find in addition to the normal pop-out many elbows followed by pop-outs, with a higher frequency of them occurring a smaller loads. The elbow before the pop-out lowers the pressure at which the pop-out occurs, and the average elbow pop-out pressures obtained were about 4.5 GPa for all cases. The normal pop-outs were found in this range to be about 6.5 GPa. As the maximum load increases, we start to find weak and kink pop-outs, as they occur at a pressure much higher than the normal pop-outs, namely around 10.5 GPa for all maximum applied loads tested. Their frequency increases with higher loads and will push the average up. Fast phase transformation upon unloading, leading to a kink pop out, may occur due to cracking and stress relaxation, which was seen at maximum applied loads higher than 35 mN. Also, the normal pop out average is seen to rise with maximum applied load as well.

For this range of maximum applied load and average unloading rates of 2, 3, and 4 nm/s, it can be seen that there is a band of permissible averages found in the data sets (Fig. 10). The width of this band is about 1.5 GPa for these three unloading rates. The results for a wider range of average unloading rates are discussed in Sec. III. E.

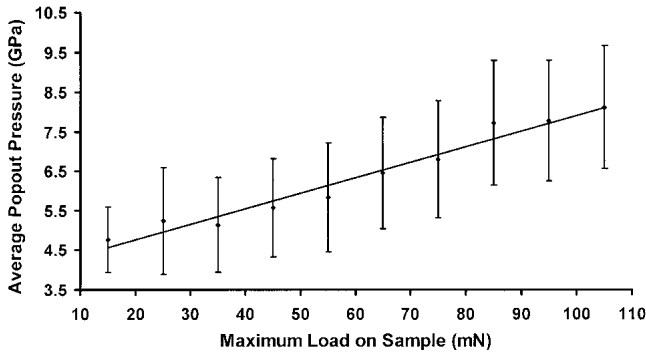


FIG. 7. Average pop-out pressures for indentations with an average unloading rate of 4 nm/s at different maximum applied loads on the sample. Error bars show the standard deviation within the data set. This graph is representative of all pop-out events, including pop-out, kink pop-out, and elbow pop-out.

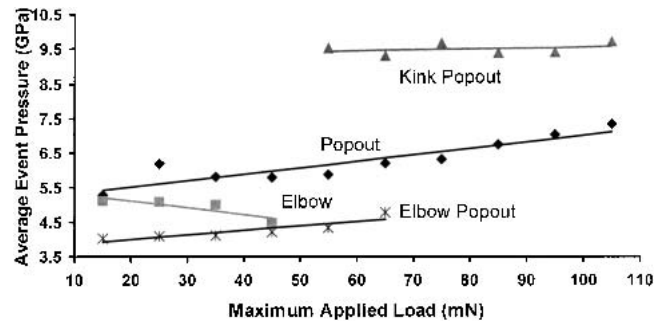


FIG. 9. Average event pressures for an average unloading rate of 4 nm/s and different maximum applied loads.

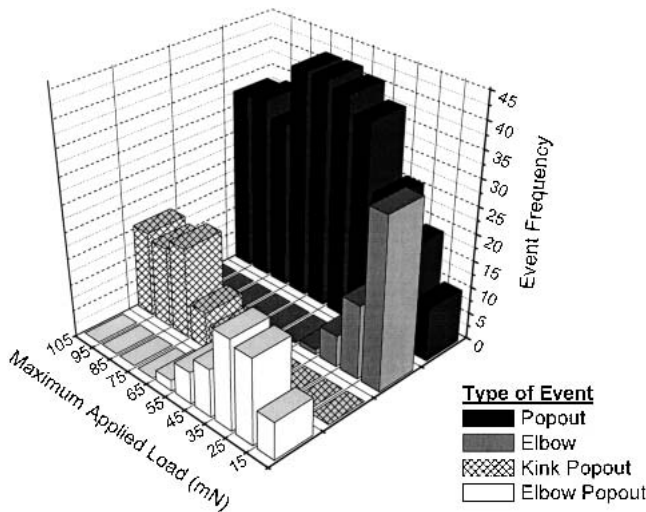


FIG. 8. Frequency of events for an average unloading rate of 4 nm/s and varying maximum applied loads.

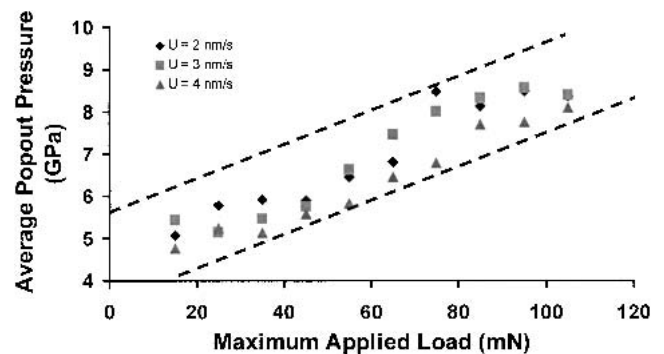


FIG. 10. Average pop-out pressure for varying maximum applied loads and average unloading rates. Si-II is stable above about 12 GPa and metastable from about 4 to 12 GPa.

E. Average event pressures for varying average unloading rates

In a similar sense, results were obtained for event pressures for varying average unloading rates with values of 1, 2, 3, 4, 5, 10, 20, and 30 nm/s and maximum applied loads of 35, 75, and 95 mN. For the 35-mN case, it was seen that the number of elbows increased with unloading speed, and not many kink pop-outs occurred over the range of unloading rates [Fig. 11(a)]. However, for the 75- and 95-mN cases, elbow events disappeared completely and only a few elbows followed by pop-out events were found at higher average unloading rates [Fig. 11(b)].

A strong trend that we see in the data is that as the unloading time for a given maximum load decreases, so does the average pressure of pop-outs occurring, again in a linear fashion (Fig. 12). When the unloading rate is quick, kinetically it has less of a chance to pop-out right

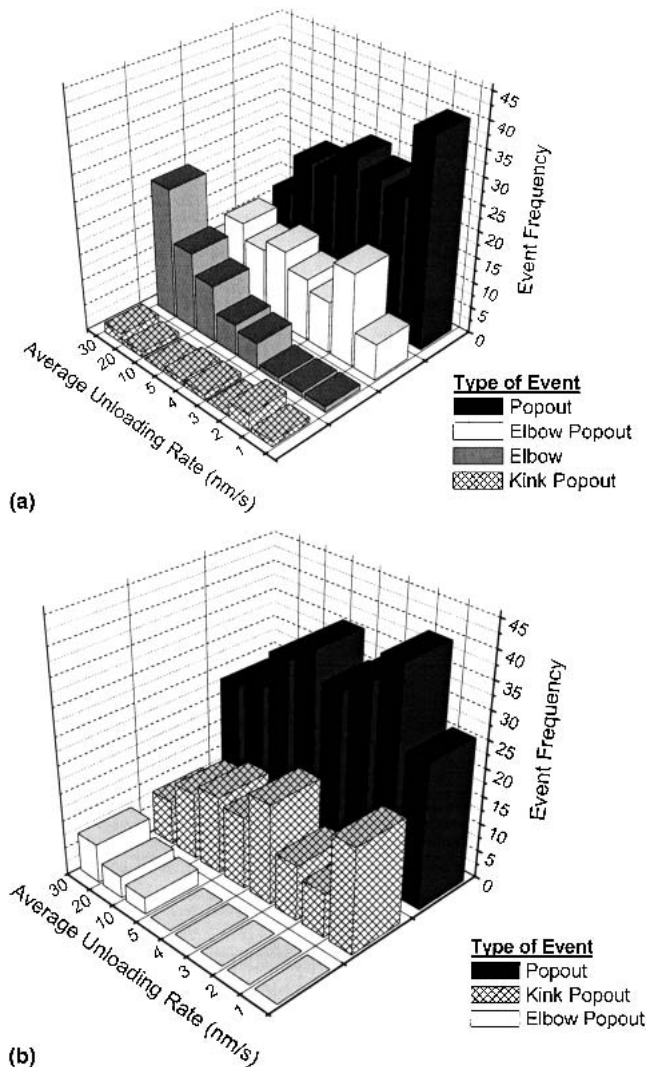


FIG. 11. Event frequency for maximum applied loads of (a) 35 mN and (b) 75 mN and various average unloading rates.

away at a high pressure and will either end up popping out at a low contact pressure or elbowing, also at a very low pressure. This should be taken as the lower limit of metastability for Si-II. For the case of the 75-mN indentations, the average pop-out pressure was close to 9 GPa

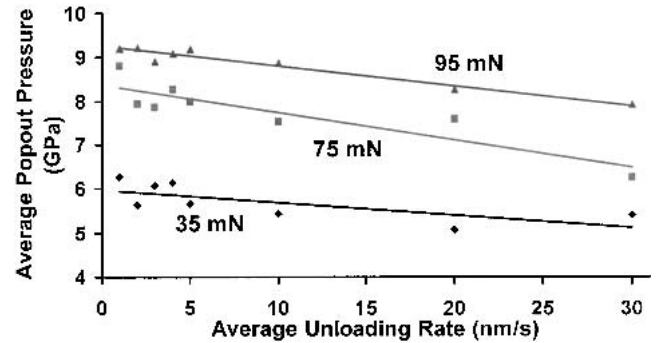


FIG. 12. Dependence of average pop-out pressure with varying average unloading rate. Points show experimental data and lines are linear fits.

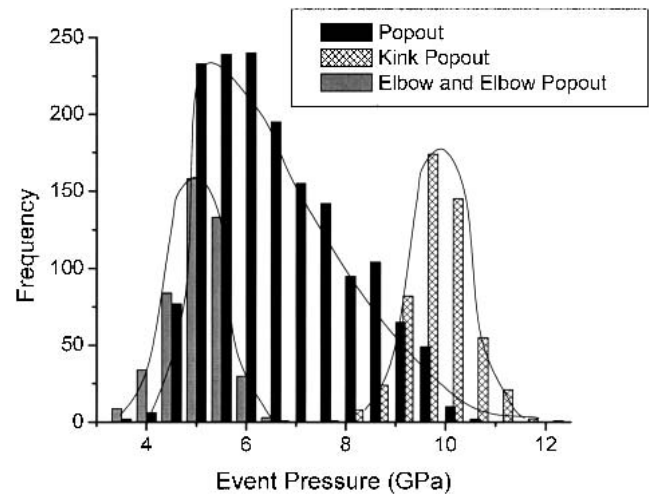


FIG. 13. Total event frequency for all indentations.

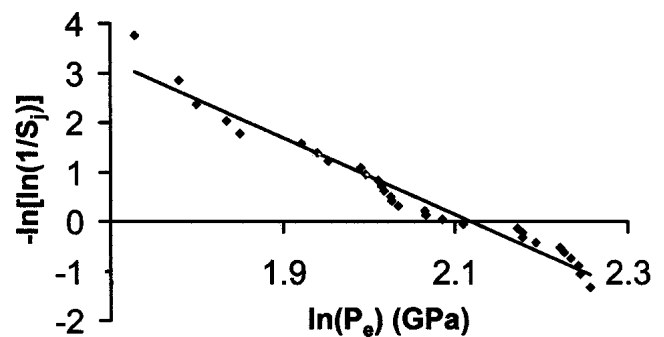


FIG. 14. Weibull fit for pop-out events at a 95 mN load and 3 nm/s unloading rate, where P_e is event pressure (GPa) and S_j is the survival probability.

TABLE II. Summary of all event statistics.

Event	Frequency	Average (GPa)	Standard deviation (GPa)	Permissible range (GPa)
Popout	1614/2581 or 62.5%	6.77	1.37	4.5–11.0
Kink pop-out	514/2581 or 19.9%	9.91	0.63	8.0–12.0
Elbow and elbow pop-out	453/2581 or 71.6%	4.67	0.56	3.5–6.5

when the average unloading rate was 1 nm/s. However, when the average unloading rate changed to 30 nm/s, the average pop-out pressure decreased to about 7 GPa. Thus, we see lower pop-out event pressures and a greater chance of elbowing at lower loads at higher average unloading rates. This is conducive with the aforementioned kinetic reasoning. When the contact area is small and the time for the Si-II to Si-III or Si-XII transformation to occur is also small, the material simply has no chance to transform to a crystalline phase, much like quenching. Instead, it is likely to form amorphous material on the surface. Since the time to load was the same for all indentations, this data shows once again that the formation of a-Si occurs through metallic Si-II^{5,13} and is not a result of pressure-induced amorphization.²⁶

F. Statistics of all events in the comprehensive data set

As can be seen in Fig. 13, at the end of calculating all event pressures for all loading and unloading conditions, the events fall into three main categories that were dependent on average contact pressure: elbow and elbow pop-out, pop-out, and kink pop-out. The elbow and elbow pop-out and kink pop-out groups were seen to have normal distributions, while the pop-out group showed a Weibull-type distribution. A Weibull fit for about 30 pop-out events for one set of indentations at 95 mN and 3 nm/s unloading rate can be seen in Fig. 14. This is evidence that the Si-II to Si-III and Si-XII transformation may be looked at statistically as a pressure to failure for the pop-out, but in other cases the transformation pressure is more or less normally distributed around a certain pressure. A summary of the frequency, average, standard deviation, and permissible range for each of the categories is found in Table II. It should be noted that it is possible that a different type of distribution might be found if different loading or unloading parameters were used, but more extensive experimentation will have to be conducted to determine this.

We may suggest at this point from the results of Raman microspectroscopy that any sort of elbow event in the unloading curve can be correlated with formation of amorphous silicon on the surface of the indentation and any sort of pop-out event can be correlated with the formation of Si-XII and Si-III. However, we have seen

that elbow events are not necessary for amorphous silicon formation, and likewise pop-out events are not necessary for Si-III and Si-XII formation. From the histogram in Fig. 13, we can deduce that amorphous silicon has a tendency to form between 4 and 6 GPa. Similarly, from the pop-out and kink pop-out trends, we may state that the formation of Si-III and Si-XII begins between 4.5 and 11.5 GPa.

IV. CONCLUSIONS

Various insights into the behavior of silicon during loading and unloading for a Berkovich or other sharp indenter were gained. We found that the maximum applied indentation load positively affects the pressure at which pop-out events occur. It was seen by Raman microspectroscopy that primarily amorphous silicon is on the surface (<0.1 to 0.2 μm) of elbow and elbow followed by pop-out event indentations, but there is a presence of Si-III and Si-XII at greater depths (up to 1 μm). In all cases, it has been found that these transformations are all brought about by nonequilibrium mechanisms. It is reasoned because there has been no evidence from Raman microspectroscopy or TEM work that has been done to suggest a presence of Si-I directly on the surface of the indented area. Pop-out and kink pop-out events show a strong presence of Si-III and Si-XII on the surface and below it. The distinctive shape of the kink pop-out was found to possibly be due to the effect of phase transformations combined with cracking around indentations with higher maximum applied loads (>45 mN). Quicker unloading rates were found to lower the pressure at which pop-out events occur, as well as increase the chance of elbow events and amorphous silicon formation. Finally, over a range of conditions, we have established an experimental threshold for the contact pressures at which kink pop-outs, elbow and elbow pop-outs, and pop-outs can occur.

ACKNOWLEDGMENTS

This work was funded by the National Science Foundation (NSF) through Grant Nos. DMR-0196424 and DMI-0196360. The authors would like to thank Mr. D. Ge for his thoughts and ideas that contributed to this publication.

REFERENCES

1. V. Domnich and Y. Gogotsi, *Rev. Adv. Mater. Sci.* **3**, 1 (2002).
2. E.R. Weppelmann, J.S. Field, and M.V. Swain, *J. Mater. Res.* **8**, 830 (1993).
3. S.V. Hainsworth, A.J. Whitehead, and T.F. Page, in *Plastic Deformation of Ceramics*, edited by J.L. Routbort (Plenum Press, New York, 1995), p. 173.
4. J.S. Williams, Y. Chen, J. Wong-Leung, A. Kerr, and M.V. Swain, *J. Mater. Res.* **14**, 2338 (1999).
5. V. Domnich, Y. Gogotsi, and S. Dub, *Appl. Phys. Lett.* **76**, 2214 (2000).
6. E.R. Weppelmann, J.S. Field, and M.V. Swain, *J. Mater. Sci.* **30**, 2455 (1995).
7. Y.G. Gogotsi, V. Domnich, S.N. Dub, A. Kailer, and K.G. Nickel, *J. Mater. Res.* **15**, 871 (2000).
8. J.E. Bradby, J.S. Williams, J. Wong-Leung, M.V. Swain, and P. Munroe, *J. Mater. Res.* **16**, 1500 (2001).
9. J.Z. Hu, L.D. Merkle, C. S. Menoni, and I.L. Spain, *Phys. Rev. B* **34**, 4679 (1986).
10. J.Z. Hu and I.L. Spain, *Solid State Commun.* **51**, 263 (1984).
11. W.W. Gerberich, J.C. Nelson, E.T. Lilleodden, P. Anderson, and J.T. Wyrobek, *Acta Mater.* **44**, 3585 (1995).
12. J.E. Bradby, J.S. Williams, J. Wong-Leung, M.V. Swain, and P. Munroe, *Appl. Phys. Lett.* **77**, 3749 (2000).
13. A. Kailer, Y.G. Gogotsi, and K.G. Nickel, *J. Appl. Phys.* **81**, 3057 (1997).
14. J. Crain, G.J. Ackland, J.R. Maclean, R.O. Piltz, P.D. Hatton, and G.S. Pawley, *Phys. Rev. B* **50**, 13043 (1994).
15. Y. Gogotsi, S. Welz, D. Ersoy, and M.J. McNallan, *Nature* **411**, 283 (2001).
16. A.V. Kulkarni and B. Bhushan, *Thin Solid Films* **290**, 206 (1996).
17. I. Zarudi and L.C. Zhang, *Tribology Int.* **32**, 701 (1999).
18. W.C. Oliver and G.M. Pharr, *J. Mater. Res.* **7**, 1564 (1992).
19. N.V. Novikov, S.N. Dub, Y.V. Milman, I.V. Gridneva, and S.I. Chugunova, *J. Superhard Mater. (Sverkhтвердые Materialy)* **18**, 32 (1996).
20. I.N. Sneddon, *Int. J. Eng. Sci.* **3**, 47 (1965).
21. J.L. Hay and G.M. Pharr, in *Mechanical Testing and Evaluation*, edited by D. Medlin (ASM International, Materials Park, OH, 2000), Vol. 8, p. 232.
22. M. Hanfland and K. Syassen, *High Pressure Res.* **3**, 242 (1990).
23. D.E. Carlson and C.R. Wronski, in *Amorphous Semiconductors*, edited by M.H. Brodsky (Springer, New York, 1979), p. 287.
24. L.C. Zhang and I. Zarudi, *Int. J. Mech. Sci.* **43**, 1985 (2001).
25. T.D. Shen, C.C. Koch, T.L. McCormick, R.J. Nemanich, J.Y. Huang, and J.G. Huang, *J. Mater. Res.* **10**, 139 (1995).
26. V.V. Brazhkin, A.G. Lyapin, S. V. Popova, and R.N. Voloshin, *Phys. Rev. B* **51**, 7549 (1995).